





# Phosphorylation of myosin A regulates gliding motility and is essential for *Plasmodium* transmission

Johanna Ripp<sup>1</sup> , Xanthoula Smyrnakou<sup>1,†</sup>, Marie-Therese Neuhoff<sup>ff1</sup> , Franziska Hentzschel<sup>1,2</sup>  & Friedrich Frischknecht<sup>1,2,\*</sup> 

## Abstract

Malaria-causing parasites rely on an actin–myosin-based motor for the invasion of different host cells and tissue traversal in mosquitoes and vertebrates. The unusual myosin A of *Plasmodium* spp. has a unique N-terminal extension, which is important for red blood cell invasion by *P. falciparum* merozoites *in vitro* and harbors a phosphorylation site at serine 19. Here, using the rodent-infecting *P. berghei* we show that phosphorylation of serine 19 increases ookinete but not sporozoite motility and is essential for efficient transmission of *Plasmodium* by mosquitoes as S19A mutants show defects in mosquito salivary gland entry. S19A along with E6R mutations slow ookinetes and salivary gland sporozoites in both 2D and 3D environments. In contrast to data from purified proteins, both E6R and S19D mutations lower force generation by sporozoites. Our data show that the phosphorylation cycle of S19 influences parasite migration and force generation and is critical for optimal migration of parasites during transmission from and to the mosquito.

**Keywords** malaria; mosquito; myosin; ookinete; sporozoite

**Subject Categories** Cell Adhesion, Polarity & Cytoskeleton; Microbiology, Virology & Host Pathogen Interaction; Post-translational Modifications & Proteolysis

**DOI** 10.15252/embr.202254857 | Received 14 February 2022 | Revised 6 April 2022 | Accepted 8 April 2022 | Published online 4 May 2022

**EMBO Reports (2022) 23: e54857**

## Introduction

Apicomplexan parasites rely on an actin–myosin-based motor for migration on and through tissues and for cell invasion (Heintzelman, 2015; Frénel *et al.*, 2017). Compared with canonical actin–myosin motors, however, apicomplexans have evolved an intriguingly divergent machinery reliant on short and highly dynamic actin

filaments and unique class XIV myosins, which lack the extended cargo-binding tail domain (Herm-Götz *et al.*, 2002; Bookwalter *et al.*, 2017; Douglas *et al.*, 2018; Robert-Paganin *et al.*, 2019). As key parts of the motor, actin 1 and myosin A (MyoA) are essential in *Plasmodium* spp., the causative agents of malaria in vertebrates (Bushell *et al.*, 2017). Malaria is caused by the exponential replication of parasites in red blood cells. Red blood cells are invaded by otherwise largely non-migrating extracellular *Plasmodium* merozoites in an actin–myosin-dependent way (Mizuno *et al.*, 2002; Das *et al.*, 2017; Robert-Paganin *et al.*, 2019; Blake *et al.*, 2020). Mammal-infecting *Plasmodium* parasites undergo a complex life cycle that relies on *Anopheles* mosquitoes as disease vectors (Douglas *et al.*, 2015). Indeed, *Plasmodium* parasites likely evolved in insects before they spread to vertebrate hosts, suggesting that the core machinery of the parasite has initially adapted to a life in insects (Poinar, 2016). Within the mosquito, two highly motile extracellular forms of the parasite also rely on the actin–myosin motor. In the mosquito gut, ookinetes are formed and migrate across the midgut epithelium to transform into oocysts. In those oocysts, sporozoites are formed (Angrisano *et al.*, 2012b). Sporozoites need motility to egress from oocysts, enter salivary glands, migrate in the skin, enter and exit the bloodstream and to infect hepatocytes (Fig 1A). This formidable journey likely requires a higher level of regulation of the actin–myosin motor compared with merozoites. Indeed, several actin regulatory proteins are only found to be important in sporozoites and mutations in actin or actin-binding proteins could be identified that only impact sporozoite motility with little impact on merozoites or ookinetes (Ganter *et al.*, 2009; Bane *et al.*, 2016; Moreau *et al.*, 2017; Douglas *et al.*, 2018). Furthermore, MyoA and other components of the gliding machinery are phosphorylated in blood stages, ookinetes, and sporozoites, suggesting that phosphorylation regulates motility (Sebastian *et al.*, 2012; Alam *et al.*, 2015; Lasonder *et al.*, 2015; Swearingen *et al.*, 2017).

Many insights into the function of the apicomplexan actin–myosin motor and its associated proteins have been gained from the study of *Toxoplasma gondii*, a highly successful parasite circulating

<sup>1</sup> Integrative Parasitology, Center for Infectious Diseases, University of Heidelberg Medical School, Heidelberg, Germany

<sup>2</sup> German Center for Infection Research, DZIF Partner Site Heidelberg, Heidelberg, Germany

\*Corresponding author. Tel: +49-6221-566537; Fax: +49-6221-564643; E-mail: freddy.frischknecht@med.uni-heidelberg.de

<sup>†</sup>Present address: Gene Therapy for Hearing Impairment and Deafness, Department of Otolaryngology, Head & Neck Surgery, University of Tübingen Medical Center, Tübingen, Germany

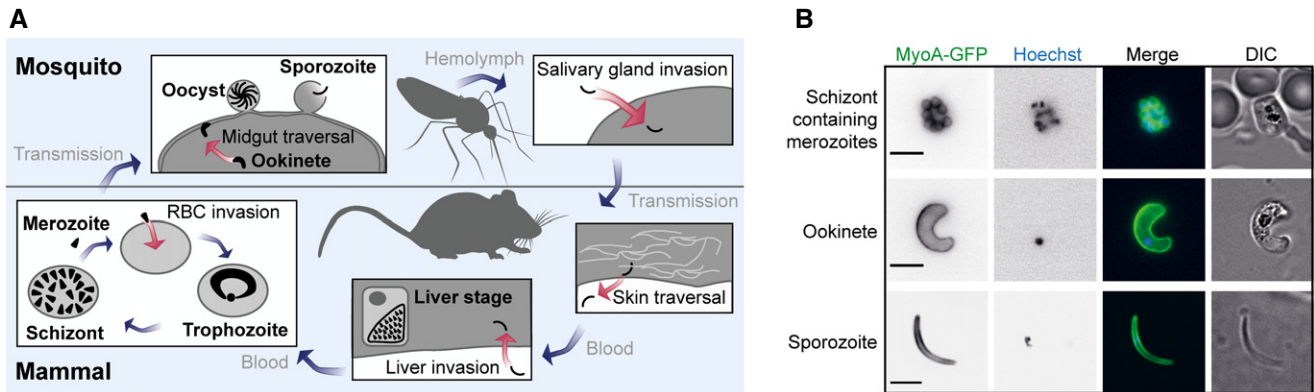


**Figure 1. Myosin motor is required at multiple stages throughout the *Plasmodium* life cycle.**

- A** When an *Anopheles* mosquito feeds from an infected mammal, it takes up parasites with the bloodmeal. The parasites transform into motile ookinetes in the midgut. Myosin is essential for traversal of the midgut epithelium. Ookinetes transform into oocysts and develop into hundreds of sporozoites. Sporozoites egress from oocysts to float in the hemolymph. Active motility allows sporozoites to invade the salivary glands from where they are transmitted into the skin with the next bite. They traverse the skin and enter into a blood vessel. With the bloodstream, they are transported until they reach the liver and actively invade a hepatocyte to develop into thousands of merozoites. These merozoites are released back into the bloodstream where they depend on myosin to actively invade red blood cells (RBCs) and multiply. Red and blue arrows indicate active and passive movements of the parasite, respectively.
- B** The motor protein MyoA localizes to the periphery of motile *Plasmodium* stages. Images show parasites expressing GFP-tagged MyoA. Nuclei were stained with Hoechst. Scale bars, 5  $\mu\text{m}$ .

between cats and their prey but also infecting about one third of the world's human population (Frénel *et al*, 2017). For practical reasons, most studies on *T. gondii* are limited to tissue culture migration and invasion assays and it is important to note that the common ancestor of *T. gondii* and *Plasmodium* spp. split about 350–820 Mio years ago (Sato, 2011). Yet, both parasites and most apicomplexans feature similarly designed highly polarized invasive forms featuring a namesake complex apical end where vesicles fuse with the plasma membrane to secrete proteins or deposit them into the plasma membrane (Frénel *et al*, 2017). The plasma membrane is subtended by a membrane organelle called the inner membrane complex (IMC), which is the defining structure of the alveolates, the superphylum of organisms the apicomplexans belong to. On the cytoplasmic face of the IMC, a complex and stable membrane-associated network, the subpellicular network, is giving the parasites their shape (Harding & Frischknecht, 2020). In the narrow space (30 nm) between plasma membrane and IMC, the actin–myosin motor is located (Heintzelman, 2015; Frénel *et al*, 2017). Actin filaments are likely polymerized by formins located at the apical end of the parasites (Baum *et al*, 2008; Douglas *et al*, 2018; Tosetti *et al*, 2019). MyoA is anchored into the IMC by light chains and so-called gliding associated proteins (GAPs) and can move actin filaments from the front to the rear (Heintzelman, 2015; Frénel *et al*, 2017). As the actin filaments bind receptors spanning the plasma membrane, these receptors are moved rearwards. If the receptors engage with ligands on the surface of a cell, tissue, or glass coverslip, the parasite moves forward. While actin filaments could not yet be clearly shown between IMC and plasma membrane in extracellular *Plasmodium* stages (Kudryashev *et al*, 2010; Angrisano *et al*, 2012a; Siden-Kiamos *et al*, 2012), MyoA has been localized to the IMC of all invasive stages through the expression of a GFP-fusion protein (Wall *et al*, 2019; Fig 1B).

Conditional deletion of *myoA* or *actin* in *T. gondii* showed a dramatic decrease in both tachyzoite motility and cell invasion

(Meissner *et al*, 2002; Andenmatten *et al*, 2013; Egarter *et al*, 2014). Replacing the *myoA* promoter with a promoter that is only active in blood stages in the rodent-infecting malaria parasite *P. berghei* showed that ookinetes are still formed but cannot migrate in the absence of MyoA (Siden-Kiamos *et al*, 2011). Conditional mutations in MyoA and a myosin light chain in *P. falciparum* revealed an orchestrated need for merozoite force production to enter red blood cells (Blake *et al*, 2020). Crystal structures of *P. falciparum* MyoA showed that interaction sites formed by E6 and phosphorylated S19 in the N-terminal extension are important for MyoA kinetics (Robert-Paganin *et al*, 2019; Moussaoui *et al*, 2020). Mutations of these amino acids leading to the disruption of the respective interactions reduced the speed at which purified MyoA transports actin filaments *in vitro* but increased maximal force production (Robert-Paganin *et al*, 2019; Moussaoui *et al*, 2020). This suggests that phosphorylation of S19 is required for maximum myosin velocity and might hence play a role in ookinetes or sporozoites that rely on motility for much longer periods than merozoites. In laboratory settings, the major human-infecting *P. falciparum* is usually studied in cultured blood cells, while for the study of mosquito transmission the rodent malaria parasite *P. berghei* is used for reasons of experimental ease, ethical limitations, and safety (Matz & Kooij, 2015). In order to probe the role of the N-terminal extension of MyoA for ookinete and sporozoite motility, we sought to generate parasite lines of *P. berghei* that harbor different mutations in MyoA and analyze their effects in the mosquito stages. We show that the endogenous 3' untranslated region (UTR) of *myoA* is important for expression in sporozoites limiting gene modifications by classic homologous recombination. Consistent with data from *P. falciparum*, we find that the N-terminal extension is essential for blood stages. However, point mutations of E6 and S19 yielded viable parasite lines that can infect mosquitoes at normal levels despite significantly influencing ookinete migration. Strikingly, parasites expressing S19A but not the phosphomimetic S19D showed reduced mosquito salivary gland colonization and

liver infection, suggesting that phosphorylation of S19 is essential for efficient transmission.

## Results

### Exchange of 3'myoA by 3'dhfs leads to reduced myoA expression levels resulting in a defect in salivary gland invasion

To understand how single amino acid residues contribute to the function of MyoA, we first attempted to use conventional gene editing of the *myoA* locus, which results in the integration of the 3'UTR of *dhfs* and a selection cassette downstream of *myoA* (Appendix Fig S1A). This would allow insertions of mutations similar to what was achieved in our study on the actin-binding proteins coronin and profilin (Bane et al, 2016; Moreau et al, 2017). Along

with the generation of the control line, we also tested whether the *P. falciparum* orthologue can complement the function of *P. berghei* MyoA (PbMyoA; PBANKA\_1355700) by replacing PbMyoA with *P. falciparum myoA* (PfMyoA; PF3D7\_1342600). In addition, we C-terminally tagged the protein with GFP for localization studies (Fig 2A and Appendix Fig S1B and C). To test whether the clonal lines proceed through the life cycle, a prerequisite for the mutagenesis study, we analyzed all life cycle stages. While the blood stage growth rate of the PbMyoA 3'dhfs and PbMyoA-GFP 3'dhfs parasite lines were similar to wild type (wt), it was significantly reduced from ninefold per day in wt to sixfold per day in the PfMyoA 3'dhfs line (Fig 2B). To assess the ability of parasites to infect mosquitoes, we counted the numbers of oocysts that formed in the mosquito midguts 10–14 days after the insects took a blood meal on infected mice. All parasite lines could form oocysts, but the PbMyoA 3'dhfs and PfMyoA 3'dhfs lines showed significantly reduced numbers of

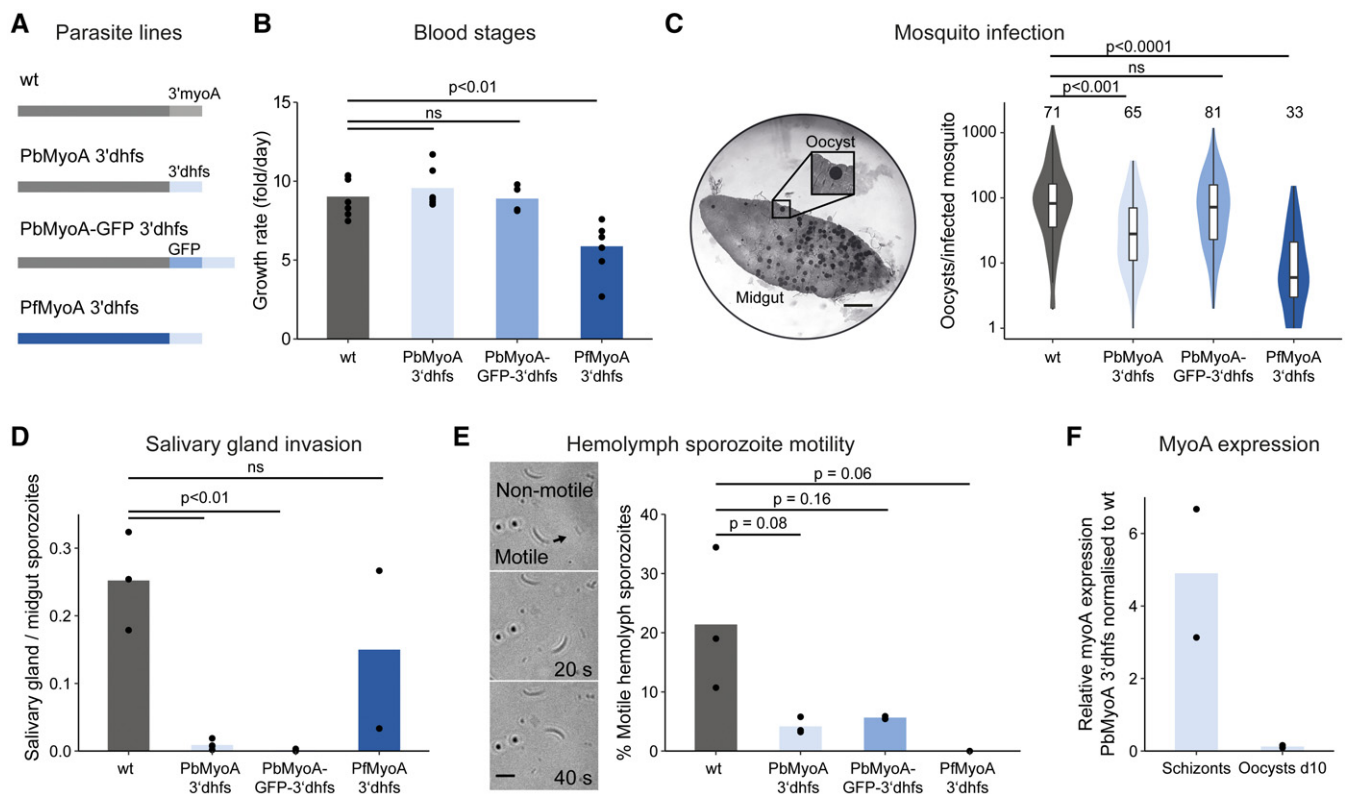


**Figure 2. Effect of 3'UTR replacement of *myoA* by the 3'UTR of *dhfs* on life cycle progression and *myoA* expression.**

- A Scheme showing simplified *myoA* loci in transgenic parasite lines.
- B Blood stage growth rate of mutated parasite lines. A single parasite was injected *i.v.* into a mouse, and the growth rate was calculated from parasitemia at day 6–9 for each mouse (black dots). Bars represent the mean of 4–7 mice.
- C Infected midgut showing oocysts stained with mercurochrome; scale bar, 200  $\mu$ m. The graph shows oocyst numbers per infected mosquito. Numbers of mosquitoes that were analyzed are indicated above the graph. Data derived from at least two independent cage feeds originating from independently infected mice. Box-and-whisker plots depict the 25% quantile, median, 75% quantile, and nearest observations within 1.5 times the interquartile range (whiskers).
- D Ratio of salivary gland to midgut sporozoites of the indicated parasite lines. Black dots: individual experiments with 10–20 mosquitoes. Bars: mean.
- E Hemolymph sporozoites were isolated and observed on glass slides by live cell imaging. Arrow indicates direction of a motile sporozoite. The graph shows the fraction of motile hemolymph sporozoites. Black dots: individual experiments with 10–20 mosquitoes. Bars: mean.
- F qRT-PCR analysis of schizonts and oocysts of the PbMyoA 3'dhfs parasite line. Individual data points correspond to the mean of three technical replicates.

Data information: Significance for (B), (D), and (E) determined by one-way analysis of variance with Tukey's multiple comparison test. Significance for (C) determined by Kruskal–Wallis test with Bonferroni's multiple comparison test.

Source data are available online for this figure.

oocysts (Fig 2C). In line with the very low number of oocysts, the number of sporozoites that formed in midgut oocysts was most reduced in the PfMyoA 3'dhfs line (Table 1). In contrast, PbMyoA 3'dhfs and PbMyoA-GFP 3'dhfs sporozoite numbers within oocysts were similar to wt. However, sporozoite numbers from salivary glands were strongly reduced, suggesting a defect in salivary gland invasion (Table 1 and Fig 2D). Surprisingly, the ratio of salivary gland to midgut sporozoites was similar to wt in the PfMyoA 3'dhfs parasite line. Next, we examined whether the defect in salivary gland invasion could be due to reduced motility of sporozoites floating in the hemolymph, the circulating fluid of the mosquito. Indeed, a much lower fraction of isolated hemolymph sporozoites displayed gliding motility on glass in these parasite lines (Fig 2E). We hypothesized that the defect in *in vitro* motility and salivary gland invasion might be due to a difference in *myoA* expression resulting from the replaced 3'UTR. Indeed, quantification of *myoA* mRNA levels via qPCR revealed a five- to tenfold reduction in the PbMyoA 3'dhfs line in early oocysts, while there was increased *myoA* expression in schizonts (Fig 2F). Hence, a different strategy for mutagenesis was needed that kept the endogenous 3'UTR of *myoA* intact.

### Phosphorylation of MyoA at serine 19 modulates blood stage growth and ookinete migration

In order to leave the 3'UTR within the *myoA* locus intact, we next used a cloning strategy that resulted in selection marker-free parasite lines (Lin *et al.*, 2011). In the first step, we generated a clonal *ama1* promoter swap parasite line (Appendix Fig S2A and B). This choice was motivated by the prior successful promoter swap, where the *myoA* promoter was changed to the *ama1* promoter and shown to arrest ookinete motility (Siden-Kiamos *et al.*, 2011). In a second step, we replaced the *ama1* promoter by the endogenous *myoA* promoter and the *myoA* ORF carrying the mutation of interest at the 5' end of *myoA*. As a control, we reconstituted the wild-type (wt) *myoA* locus (Appendix Fig S2C and E). This resulted in control parasites proceeding through the life cycle as anticipated (Table 1). To assess the role of the unique N terminus of MyoA on parasite motility, we focused on two amino acids, E6 and S19, which are thought

to be especially important as they interact with switch I/II and the converter, respectively, and are required to transport actin filaments at maximum speed (Robert-Paganin *et al.*, 2019; Moussaoui *et al.*, 2020) (Fig 3A). To this end, we introduced a reverse charge at position 6 (mutant E6R) and replaced serine at position 19 with either a phosphorylation incompatible alanine (mutant S19A) or a phosphomimetic aspartate (mutant S19D) (Fig 3B). Previous data suggest that the S19A mutant would only have a minor impact on merozoites but affect the fast gliding stages (Robert-Paganin *et al.*, 2019; Blake *et al.*, 2020). To study the overall importance of the N-terminal extension, we also generated a construct aiming to delete the first 19 amino acids from the N terminus of MyoA (Fig 3B). While we obtained parasites with the point mutations after transfection, we failed to delete the N-terminal extension in four attempts, suggesting that this part of the protein is essential. Interestingly, the growth of E6R and S19A mutants was not significantly different from wild type, although S19A showed in three out of four infections a lower infection rate. Intriguingly, S19D parasites grew consistently slower in the blood (Fig 3C). We next investigated the transmission of the different lines into mosquitoes. We could not detect a difference in exflagellation of gametocytes and ookinete formation but strikingly found differences in ookinete motility. Quantification of the different parasite lines revealed that, compared with the wt and wt reconstituted line, a higher proportion of S19D-expressing ookinetes migrated (Fig 3D). While there was no difference in ookinete migration speed between WT and the WT reconstituted line, E6R and S19A expressing lines moved slower and S19D moved faster (Fig 3E). Ookinetes move in different fashions either on circular or meandering paths (Appendix Fig S3A; Movie EV1). We found that S19D ookinetes showed a larger proportion of parasites migrating in a mixed pattern during which ookinetes switch between a circular and meandering path (Appendix Fig S3B). This likely is due to the higher speed of S19D ookinetes, which allows them to cover a longer distance during the observed period, increasing the likelihood of switching the migration pattern. This difference in speed, however, did not translate in a different efficiency of colonization of the mosquito midgut, where we found similar numbers of oocysts for all lines (Fig 3F).

**Table 1. Mosquito infection capacity of the different parasite lines.**

| Parasite line     | Infection rate [%] (n) | MG sporozoites/inf mosquito (n) | HL sporozoites/inf mosquito (n) | SG sporozoites/inf mosquito (n) |
|-------------------|------------------------|---------------------------------|---------------------------------|---------------------------------|
| wt                | 80 ± 10 (85)           | 76,000 ± 42,000 (90)            | 3,000 ± 100 (37)                | 20,000 ± 14,000 (50)            |
| PbMyoA 3'dhfs     | 60 ± 20 (127)          | 83,000 ± 34,000 (123)           | 6,300 ± 3,400 (61)              | 700 ± 800 (59)                  |
| PbMyoA-GFP 3'dhfs | 80 ± 20 (115)          | 89,000 ± 57,000 (59)            | n.d.                            | <b>100 ± 100</b> (57)           |
| PfMyoA 3'dhfs     | 50 ± 20 (73)           | <b>7,500 ± 6,400</b> (60)       | n.d.                            | <b>600 ± 300</b> (56)           |
| RL                | 0 (40)                 | n.d.                            | n.d.                            | n.d.                            |
| wt recon          | 70 ± 20 (91)           | 84,000 ± 36,000 (74)            | 5,600 ± 1,800 (56)              | 13,000 ± 6,900 (48)             |
| MyoA E6R          | 80 ± 20 (112)          | 70,000 ± 15,000 (99)            | 4,700 ± 1,000 (51)              | 16,000 ± 7,200 (48)             |
| MyoA S19A         | 60 ± 20 (117)          | 130,000 ± 70,000 (87)           | 11,000 ± 6,900 (38)             | <b>3,900 ± 2,600</b> (48)       |
| MyoA S19D         | 80 ± 10 (90)           | 78,000 ± 50,000 (104)           | 4,300 ± 1,800 (49)              | 10,000 ± 2,600 (54)             |

Infection rate, numbers of infected mosquitoes after a cage feed. *n*, numbers of mosquitoes investigated. Note that sporozoite numbers are from at least two different cage feeds determined from pooled organs. Significant reductions are shown in bold.



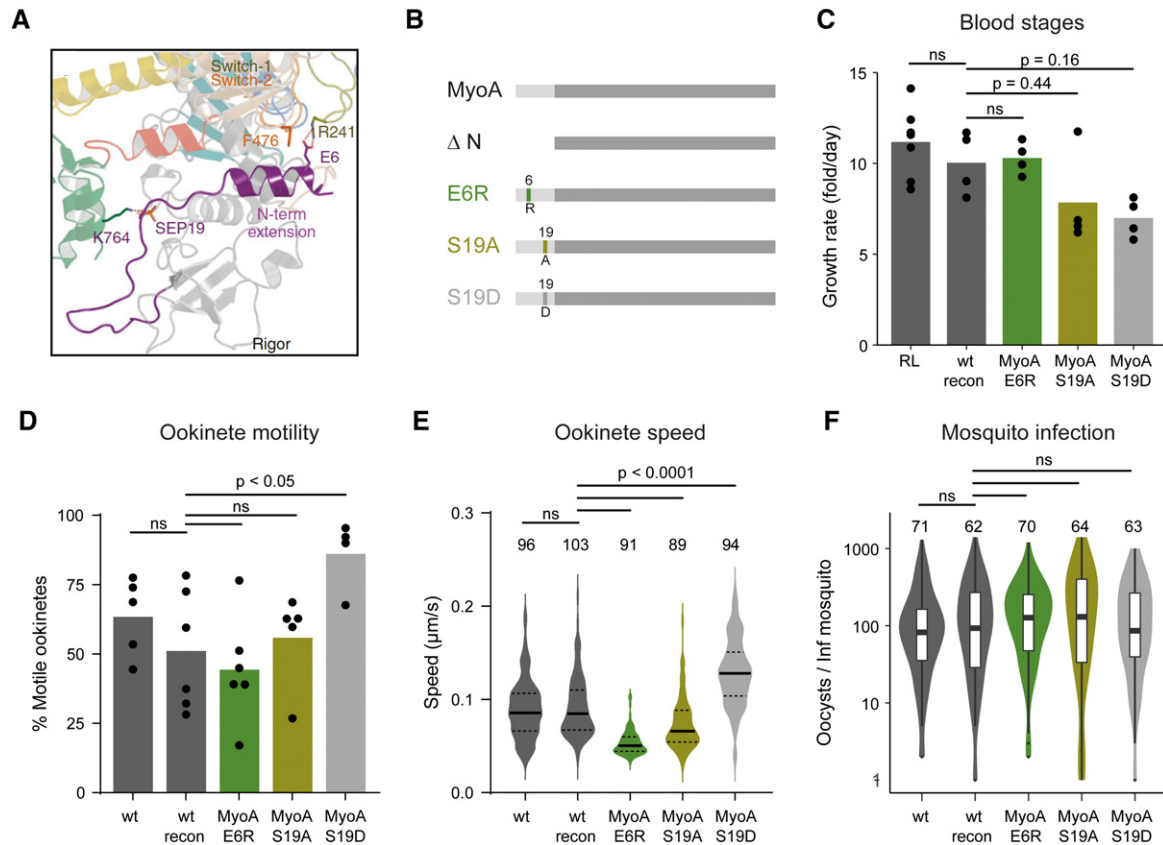


**Figure 3. Phosphorylation of MyoA at serine 19 is important for ookinete motility.**

**A** Zoom of the PfMyoA structure showing important amino acid interactions for stabilization of the rigor-like state that are thought to influence the kinetic properties of MyoA. The N-terminal extension is depicted in purple. It is located in proximity to Switch I (green) and the connectors Switch II (orange) and Relay (yellow). Phosphorylated serine 19 (SEP19) in the N-terminal extension interacts with lysine 764 (K764) in the converter and glutamic acid 6 (E6) in the N-terminal extension interacts with arginine 241 (R241) and phenylalanine 476 (F476) from switch I and II. Image taken from Robert-Paganin et al (2019). The image was published under a Creative Commons Attribution 4.0 International License (<http://creativecommons.org/licenses/by/4.0/>).

**B** Scheme of mutated MyoA versions that are expressed in clonal parasite lines at the endogenous *myoA* locus. Either the complete N-terminal extension is deleted (19 amino acids) or point mutations within amino acids that are located in the N-terminal extension are introduced.

**C** Blood stage growth rate of clonal parasite lines. A single parasite or 100 IRBCs were injected *i.v.* into a mouse and the growth rate was calculated from parasitemia at day 6–9. Black dots: individual mice; bars: mean.

**D** Proportion of motile ookinetes. Black dots: Individual movie; bars: mean. Data pooled from three independent biological replicates with 1–3 movies taken per experiment. See also Movie EV1.

**E** Speed of ookinetes of the different lines. Numbers of analyzed parasites are shown above the graph. Data pooled from three independent experiments (biological replicates). Violin plots show median (line) and quartiles (dashed lines).

**F** Number of oocysts per infected mosquito. Numbers of analyzed mosquitoes are shown above the graph. Data pooled from at least three independent cage feeds originating from independently infected mice. Box-and-whisker plots depict the 25% quantile, median, 75% quantile, and nearest observations within 1.5 times the interquartile range (whiskers).

Data information: Statistical analysis: (C) One-way analysis of variance with Tukey's multiple comparison test. (D), (F) Kruskal–Wallis test with (D) Dunn's multiple comparisons test or (F) Bonferroni's multiple comparison test.

Source data are available online for this figure.

### Phosphorylation of MyoA at serine 19 is important for salivary gland invasion of sporozoites and efficient malaria transmission

Oocysts produced normal numbers of sporozoites in all lines, which were able to exit into the hemolymph. However, sporozoite numbers in the hemolymph were slightly enhanced in the S19A parasite line, resulting in an increase in the ratio of hemolymph to midgut sporozoites (Table 1 and Fig 4A). Far fewer sporozoites were found in salivary glands of this S19A parasite line than in the other lines (Table 1) as evidenced by a significantly lower ratio of salivary

gland to midgut sporozoites (Fig 4B). This suggests a defect of S19A sporozoites to enter into salivary glands.

Next, we tested whether the mutations within the N-terminal extension of MyoA have an effect on parasite transmission back to mice. To this end, we allowed infected mosquitoes to feed on mice. We then determined the appearance and numbers of infected red blood cells starting three days after infection to evaluate the success of parasite transmission. The S19A parasite line only infected 60% of mice (5 out of 8) via natural transmission by mosquito bite, while all other parasite lines infected 100% of mice (Table 2). Those mice

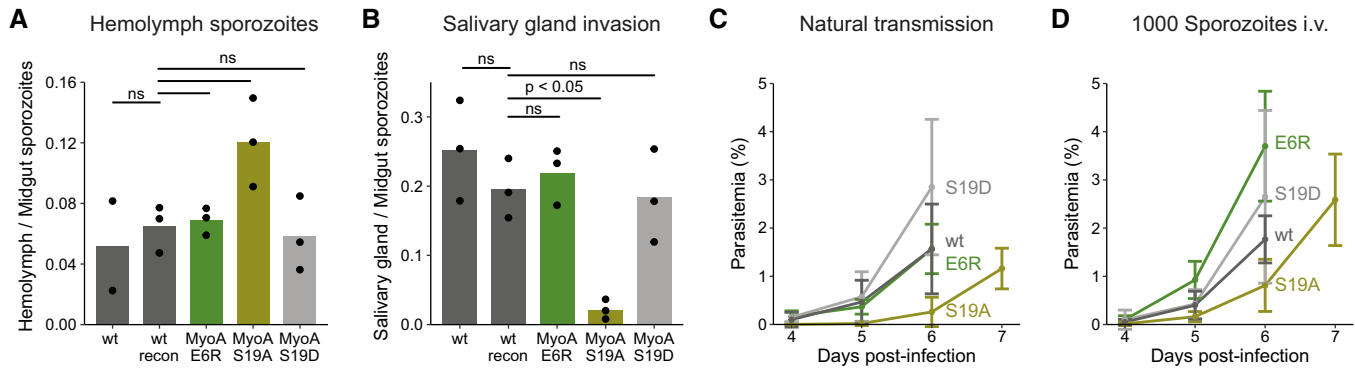


**Figure 4. Phosphorylation of MyoA at serine 19 is important for salivary gland invasion of sporozoites.**

A Ratio of hemolymph to midgut sporozoites. Black dots: individual experiments with 10–20 mosquitoes. Bars: mean.  
 B Ratio of salivary gland to midgut sporozoites. Black dots: individual experiments with 10–20 mosquitoes. Bars: mean.  
 C Blood stage infection of 3–8 mice after transmission by mosquito bite from one to two biological replicates. Shown is the mean  $\pm$  standard deviation.  
 D Blood stage infection of 4–8 mice after *i.v.* injection of 1,000 sporozoites from one to two biological replicates. Shown is the mean  $\pm$  standard deviation.

Data information: Statistical analysis: (A) and (B) One-way analysis of variance with Tukey's multiple comparison test.

Source data are available online for this figure.

**Table 2. Transmission capacity of the different parasite lines.**

| Parasite line | Natural transmission (10 mosquito bites) |                                 |               | 1,000 sporozoites <i>i.v.</i>   |                                 |               |
|---------------|--|---------------------------------|---------------|---------------------------------|---------------------------------|---------------|
|               | Prepatency                               | Parasitemia day 6               | Infected mice | Prepatency                      | Parasitemia day 6               | Infected mice |
| wt recon      | 3.8 $\pm$ 0.8                            | 1.6 $\pm$ 0.9                   | 6/6           | 3.5 $\pm$ 0.5                   | 1.8 $\pm$ 0.5                   | 6/6           |
| MyoA E6R      | 4.0 $\pm$ 0.0                            | 1.6 $\pm$ 0.5                   | 3/3           | 3.3 $\pm$ 0.5                   | 3.7 $\pm$ 1.1                   | 4/4           |
| MyoA S19A     | <b>5.0 <math>\pm</math> 0.0</b>          | <b>0.3 <math>\pm</math> 0.3</b> | <b>5/8</b>    | <b>4.1 <math>\pm</math> 0.4</b> | <b>0.8 <math>\pm</math> 0.5</b> | 8/8           |
| MyoA S19D     | 3.3 $\pm$ 0.5                            | 2.9 $\pm$ 1.4                   | 4/4           | 3.8 $\pm$ 0.5                   | 2.7 $\pm$ 1.8                   | 4/4           |

Prepatency: day after mouse infection where parasites appear for the first time in a blood smear. Significant reductions are shown in bold. Tests as in Figure 4.

that developed a blood stage infection with the S19A mutant showed a one-day delay in infection as compared to the wt control (Table 2 and Fig 4C). A one-day delay without decreased numbers of infected mice is generally considered a 90% reduction of infectivity, that is, one order of magnitude fewer infected hepatocytes (Vanderberg, 1975). These findings suggest that phosphorylation at S19 is required for efficient salivary gland invasion and efficient malaria transmission. Such a defect in natural transmission can be due to reduced numbers of sporozoites in the salivary glands, which leads to fewer transmitted sporozoites (Aleshnick *et al.*, 2020), a defect in motility in the skin or a defect in liver cell invasion (Frischknecht & Matuschewski, 2017). To test for a role in transmission and transmigration of the skin versus liver cell invasion, we intravenously injected 1,000 salivary gland-derived sporozoites. In this experiment all mice, including those infected with S19A sporozoites, became infected. This suggests that indeed the most important contribution to diminished transmission is the lower number of parasites present in the salivary gland. However, there was still a small delay in S19A infection (Table 2 and Fig 4D). To examine liver cell infection, we exposed HepG2 liver cells to WT or S19A sporozoites and investigated their capacity to form liver stages. This showed no difference in the number of infected liver cells (Appendix Fig S4A) or the size of developing liver stages between the two lines

(Appendix Fig S4B). While this does not strictly exclude that S19A mutants have a defect in liver infection, which *in vivo* is more complex than *in vitro*, the data suggest a defect in skin migration.

### Mutated MyoA affects sporozoite motility

*Plasmodium* sporozoites can migrate at more than 1  $\mu\text{m/s}$ , an order of magnitude faster than neutrophils (Vanderberg, 1974). Some even reach peak instantaneous velocities of over 5  $\mu\text{m/s}$  (Münter *et al.*, 2009). To investigate whether the defect of S19A parasites in salivary gland infection can be explained by reduced motility, we probed hemolymph and salivary gland sporozoite motility of all generated parasite lines on glass. This showed that around 20% of wt hemolymph sporozoites could migrate in the typical circular path of sporozoites or moved in a back-and-forth manner (termed patch gliding) while a reduced fraction of just 3% of S19A hemolymph sporozoites were motile (Fig 5A). The S19D mutant also showed a slight reduction of motile hemolymph sporozoites. We determined the speed of the migrating sporozoites isolated from the hemolymph and found that both S19A and S19D hemolymph sporozoites migrated significantly slower as compared to the reconstituted wt sporozoites. We next isolated sporozoites from salivary glands and imaged their migration behavior. Here, the fraction of motile E6R

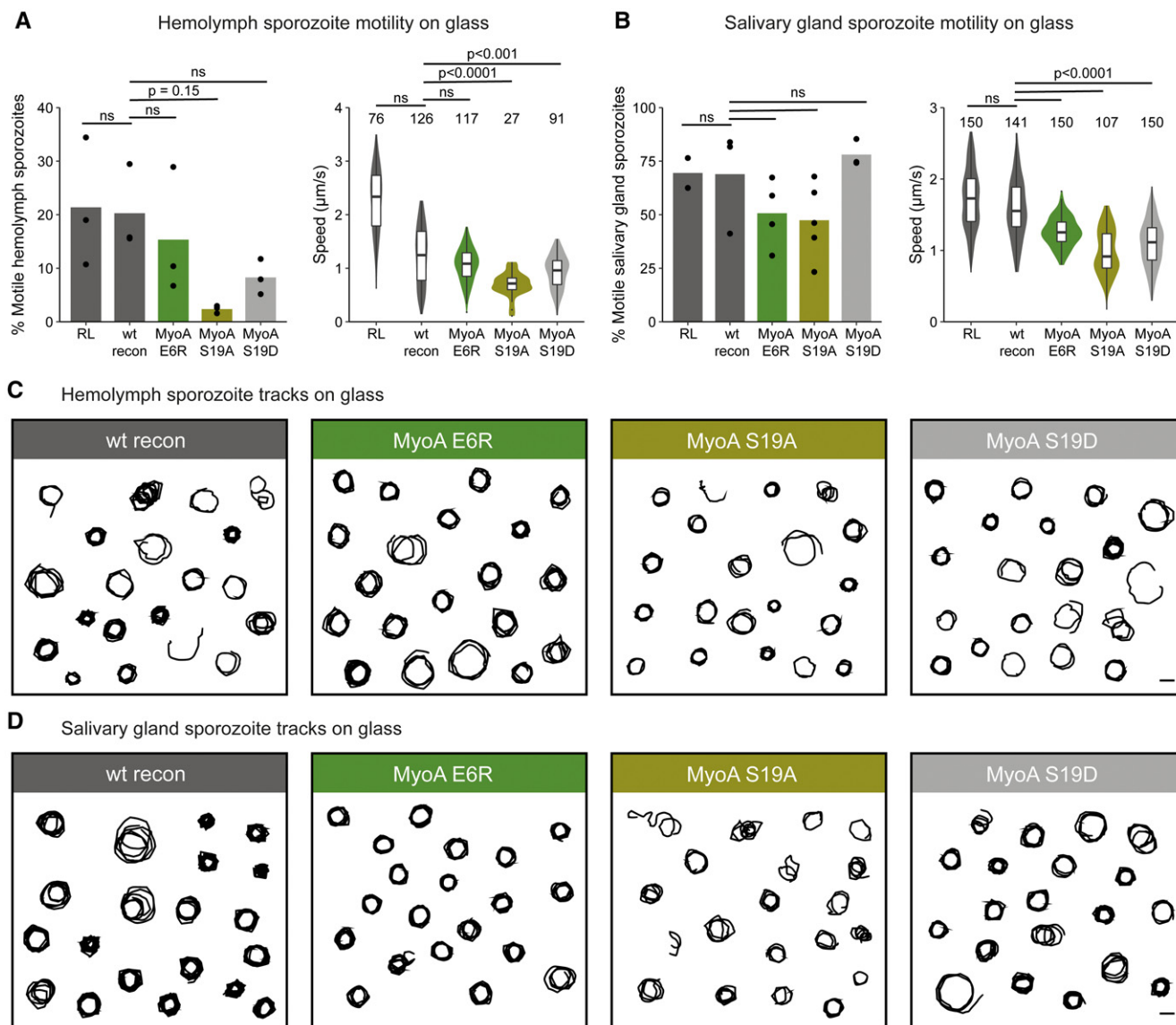


**Figure 5. Reduced speed during *in vitro* sporozoite gliding motility of parasite lines expressing mutated MyoA.**

A, B Fraction (left) and speed (right) of motile hemolymph (A) or salivary gland-derived (B) sporozoites on glass. Dots correspond to individual experiments and bars indicate the mean. Box-and-whisker plots depict the 25% quantile, median, 75% quantile, and nearest observations within 1.5 times the interquartile range (whiskers). Numbers indicate analyzed sporozoites. Significance for (A left) and (B left) determined by one-way analysis of variance with Tukey's multiple comparison test. Significance for (A right) and (B right) determined by Kruskal–Wallis test with Bonferroni's multiple comparison test.

C Selected trajectories of 20 manually tracked sporozoites isolated from hemolymph and moving over a period of 3 min. Scale bar, 10 µm.

D Selected trajectories of 20 manually tracked sporozoites isolated from salivary glands and moving over a period of 3 min. Scale bar, 10 µm.

Source data are available online for this figure.

and S19A salivary gland sporozoites was slightly lower but not significantly reduced compared to wt. However, the speed of all mutant parasites was significantly reduced as compared to wt sporozoites (Fig 5B). As some sporozoites expressing mutated actin-binding proteins alter their migration paths (Montagna et al, 2012; Bane et al, 2016), we next compared the trajectories of the migrating sporozoites from the different parasite lines. This showed no apparent difference between the mutant hemolymph and salivary gland sporozoites and the wt control parasites (Fig 5C and D).

### Changing MyoA kinetics affects sporozoite force production

Parasite motility results from a complex interplay between adhesion and force generation. Yet, force generation of sporozoites has so far only been investigated in parasites lacking either surface receptors or actin-binding proteins without a direct function in force generation (Münter et al, 2009; Hegge et al, 2012; Quadt et al, 2016; Moreau et al, 2017, 2020). Intriguingly, force generation of sporozoites was found to be lower in mutant parasites that show similar

migratory capacity or speeds as wt. To test whether mutations that are thought to impact MyoA kinetics and force generation on the molecular level result in a difference in sporozoite force production on the cellular level, we used a previously established assay based on optical tweezers (Quadt *et al*, 2016). To this end, a polystyrene bead was kept in the laser trap at a constant trapping force and positioned at the apical end of a moving salivary gland-derived sporozoite. We then investigated whether a sporozoite could pull the bead out of the trap. As we used a new commercial setup instead of the one described before (Quadt *et al*, 2016), we first calibrated the tweezers. After calibration, we repeatedly observed that around 70% of wt sporozoites were able to pull a bead out of the trap at 30 pN of force. This percentage was observed at a force of 70 pN in the previous setup (Quadt *et al*, 2016; Moreau *et al*, 2017, 2020). Currently, we do not know the source of this difference and as the previous setup was dismantled, we unfortunately cannot compare them side-by-side. Nevertheless, while about 70% of wt or wt-like

sporozoites were able to pull the bead out of the trap, only 18% of the E6R mutant and 25% of the S19D mutant were capable of pulling the bead out of the trap (Fig 6A). We were not able to perform these experiments with the phosphodeficient mutant due to the low number of S19A sporozoites in the mosquito salivary gland.

### S19A mutation diminishes 3D migration of sporozoites

We next investigated 3D motility of the mutants in polyacrylamide-based hydrogels as a model to study their migration through the skin (Ripp *et al*, 2021). To this end, dissected salivary glands were sandwiched between two hydrogels and the sporozoites released from the gland entered into the gel on corkscrew-like paths. This allowed us to also image the S19A salivary gland-derived sporozoites. Previous experiments revealed that mutant sporozoites with severe defects in 2D motility due to changes in their substrate adhesion capacity showed much improved migration capacity in 3D

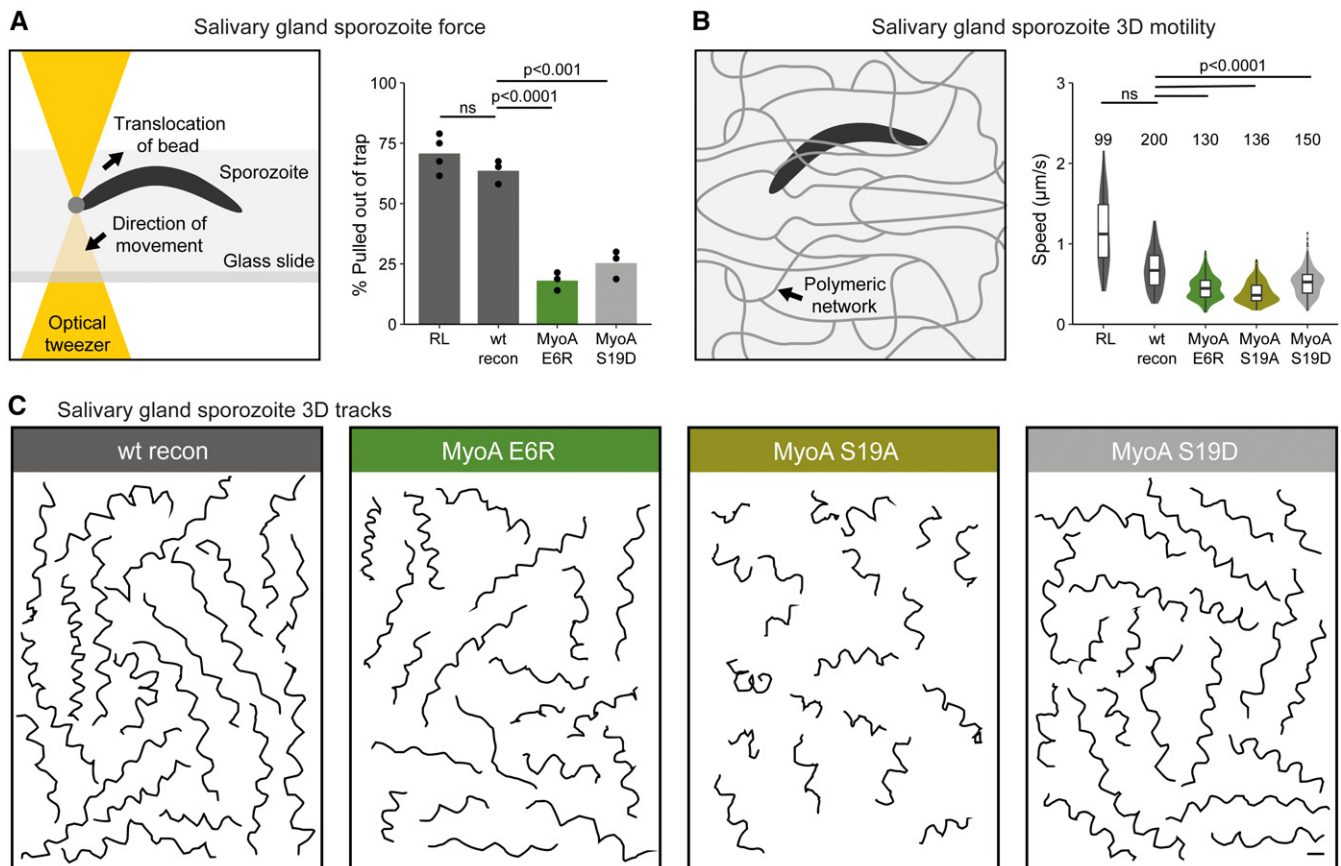


**Figure 6. Lower force generation capacity and 3D motility of parasite lines expressing mutated MyoA.**

A Scheme depicting the setup of optical tweezers for measuring the forces that a sporozoite can generate to pull a bead out of an optical trap. The bead is placed at the apical end of the sporozoite. The graph shows the fraction of sporozoites that pulled the bead out of the optical trap. Black dots: individual experiments. Bars: mean. 73–131 sporozoites were probed for each line. Significance determined by one-way analysis of variance with Tukey's multiple comparison test.

B Scheme showing a sporozoite moving through a polymeric network in 3D. The graph shows sporozoite speeds as measured by manual tracking from imaging of sporozoites in a 3D hydrogel. Box-and-whisker plots depict the 25% quantile, median, 75% quantile, and nearest observations within 1.5 times the interquartile range (whiskers). Significance determined by Kruskal–Wallis test with Bonferroni's multiple comparison test.

C Selected trajectories of 20 moving sporozoites observed over a period of 3 min. Scale bar, 10  $\mu\text{m}$ .

Source data are available online for this figure.



(Ripp et al, 2021). In contrast, the speed of all sporozoites expressing myosin mutants was significantly reduced compared with the wt-like control line (Fig 6B). The trajectories from sporozoites tracked for 3 min of observation were shorter, especially for the S19A mutant highlighting the lower displacement of these sporozoites (Fig 6C). This, along with the *in vivo* transmission data, is suggestive of a migration defect in the skin.

Taken together, these data suggest that ablating stabilizing interactions in the rigor state of MyoA results in a defect in force generation and motility at the sporozoite stage. While the E6R and S19D mutations only have a minor impact, the S19A mutation fails to efficiently enter into salivary glands. Entry into salivary glands might, therefore, constitute the strongest barrier in parasite transmission and, hence, represent the main obstacle against which the parasites needed to primarily evolve their migration and invasion machinery. Together with the data on ookinetes, we suggest that it is the turnover of phosphorylation on S19 that is important for optimal progression of the parasite along the life cycle.

## Discussion

Malaria parasites use substrate-based and myosin-powered gliding motility to enter into red blood cells, traverse the midgut epithelium, enter into salivary glands, migrate in the skin, enter and exit blood vessels, and invade hepatocytes. While entry into red blood cells is completed in < 1 min, migration in the skin can last tens of minutes and ookinetes can migrate for several hours (Gilson & Crabb, 2009; Hopp et al, 2015, 2021; Moreau et al, 2017; Ripp et al, 2021). Although invasion of the red cells appears as the most straightforward of these tasks for the parasite due to the short time and distance, recent work has shown that it presents an intriguing barrier with precise physical thresholds to be surmounted by the parasite (Blake et al, 2020; Kariuki et al, 2020). A malaria-protective polymorphism in the Dantu blood group was found to be based on an elevated mean membrane tension from 60 to 90  $\mu\text{N}/\text{m}$  with 40  $\mu\text{N}/\text{m}$  serving as a threshold above which no invasion can take place (Kariuki et al, 2020). This suggests that a large number of merozoites do not enter red cells due to this threshold. Likely, a similar phenomenon also applies for entry into salivary glands as in most mosquito infections a majority of parasites produced in the oocysts do not manage to enter into the glands. Generation of different *P. falciparum* parasite lines with mutated MyoA suggested the necessity for force generation by the merozoite in its step-wise process of red cell invasion (Blake et al, 2020). To complement the studies performed in *P. falciparum* and analyze the effect of MyoA mutations *in vivo* and throughout the whole life cycle, we generated *P. berghei* parasite lines harboring mutations within the N-terminal extension of MyoA. Subtle effects as have been seen in *P. falciparum* invasion assays were not detected during the blood stage growth of our lines, suggesting that they play comparatively minor roles *in vivo* in the rodent model. Similarly, we observed a measurable reduction in force generation by two mutants in *P. berghei* sporozoites. Interestingly, the E6R mutation caused an increase in force production *in vitro* (Moussaoui et al, 2020). While these results appear contradictory, they might not be, as an increase in force on a single-molecule level does not necessarily have to scale to an observable increase in force on the cellular level, where

multiple myosins and actin filaments come together to generate an ensemble force, which is measured in our assay (Brown & Bridgman, 2003; Quadt et al, 2016). The E6R mutation also caused a reduced speed of moving actin filaments, which might *in vivo* be correlated with a lower force. This defect, however, did not translate into a significant loss in mosquito-to-mouse transmission efficiency of the parasite lines. Only the S19A mutant line, which cannot be phosphorylated at S19 and hence alters the kinetics of the MyoA power stroke (Robert-Paganin et al, 2019), showed a dramatic reduction in the ability to transmit from mosquito to mammal (Fig 7). This block was mainly due to the incapacity of the parasites to colonize the salivary glands of the mosquito, although the parasite also showed defects in gliding in a skin-like gel and in liver infection. These results indicate that sporozoites depend on very fast myosin dynamics for efficient transmission.

Interestingly, ookinete migration is also affected by the N-terminal point mutations with E6R and S19A leading to slower and S19D to faster migration speed. While these differences in speed did not cause a change in the colonization of the gut as judged by the numbers of oocysts, one has to keep in mind that the *P. berghei*—*A. stephensi* system is essentially a laboratory model. In field situations where the numbers of oocysts are much lower, a difference in speed as measured here, could translate into a difference in gut colonization and hence affect the efficiency of transmission. Indeed, a recent modeling study suggested that an infection by two instead of one oocyst per mosquito can impact transmission by the mosquito (Churcher et al, 2017). It might, hence, be the case that the parasite is relying on different sets of phosphorylation-dephosphorylation events on myosin in its two motile mosquito stages for fine-tuning transmission to and from the mosquito.

Similar to our mutants, *T. gondii* MyoA mutants that could not be phosphorylated showed changes in the motile behavior and a decreased capacity to exit and enter cultured host cells (Tang et al, 2014). In *T. gondii*, phosphorylation of MyoA is dependent on calcium and the calcium-dependent protein kinase TgCDPK3 was identified as a kinase to phosphorylate the orthologous serine at position 20 (Tang et al, 2014; Gaji et al, 2015). Calcium is also important for the activation of *Plasmodium* sporozoite motility (Carey et al, 2014), and three CDPKs have been shown to impact sporozoite motility with two influenced by protein kinase G (Govindasamy et al, 2016; Govindasamy & Bhanot, 2020). Furthermore, S19 was predicted to be a direct substrate of PKG with S19 being a consensus phosphorylation site of PKG (Govindasamy et al, 2018). Also, S19 was identified as differentially phosphorylated in late blood stage parasites treated with the protein kinase G inhibitor “compound 2” (Alam et al, 2015). Both studies, hence, support a role for cGMP/calcium signaling in regulation of motility. Our data showing that S19 phosphorylation is important during salivary gland invasion, migration in the skin and liver invasion, suggest that similar signaling pathways play a role at different steps during malaria transmission.

Previous data from the mutagenesis of the ubiquitously expressed actin-binding protein profilin (Moreau et al, 2017, 2020) suggested a hierarchy of properties that are important for parasite transmission. The parasite can tolerate small perturbations that lead to a decrease in force generation without showing a defect in gliding motility and transmission capacity of the sporozoite (Moreau et al, 2017). Successively larger perturbations first lead to a drop in sporozoite gliding efficiency followed by a reduction in salivary gland

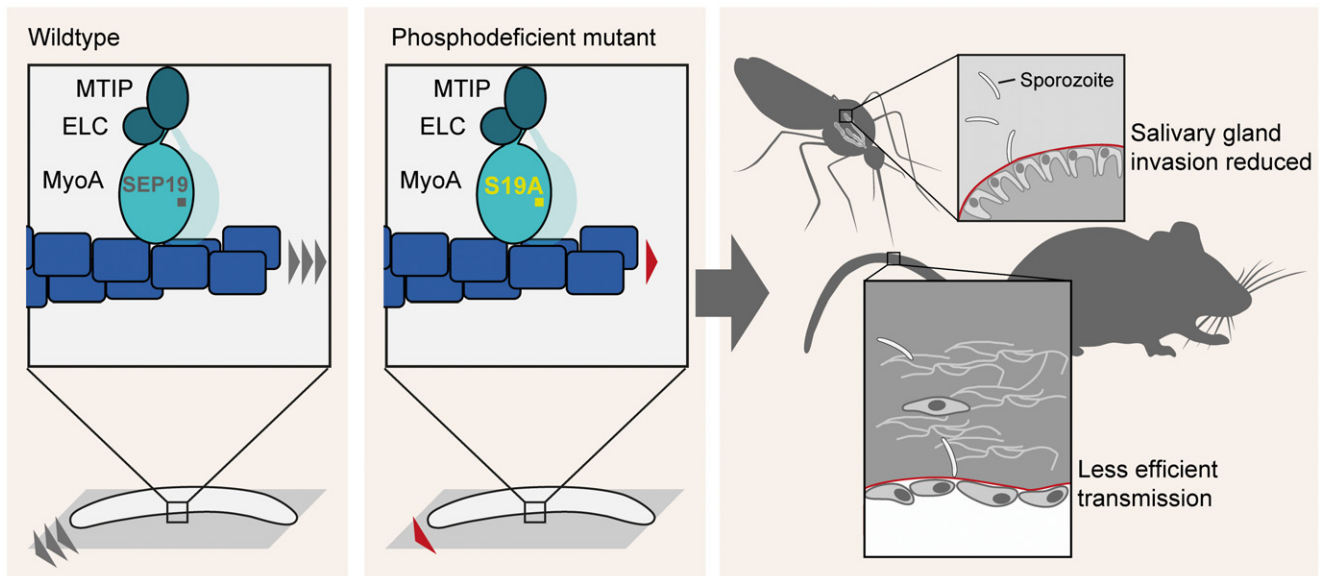


**Figure 7. Cartoon portraying importance of MyoA phosphorylation during transmission of *Plasmodium*.**

Wild-type myosin is phosphorylated in early sporozoites allowing the generation of optimal force transduction and gliding motility. Dephosphorylation is also important for optimal force generation as S19D shows lower force and speed. Non-phosphorylated myosin still allows sporozoite gliding but at reduced speed with too little force generated for efficient salivary gland invasion. Disruption of the interaction of the N terminus with the Switch I and II (E6R mutation) has similar impact as constitutive phosphorylation as mimicked by S19D.

invasion and transmission to the mammal, while ookinete motility and the infection of mosquitoes are not yet affected. Strikingly, the efficiency of mosquito colonization as measured by the presence of oocysts was not affected by specifically tuning the force generation capacity of myosin. Instead, a similar hierarchy as in the case of profilin appears with myosin mutants lacking some force generation capacity still being able to transmit efficiently, while the S19A mutant showed the largest defects in sporozoite migration and salivary gland colonization. Unfortunately, we could not measure the forces of this mutant. Nevertheless, these data might suggest that the actin–myosin motor machinery was shaped and tuned to highest efficiency by the need of the sporozoites for their long and elaborate journey from the oocysts in the mosquito midgut to the hepatocyte in a mammalian liver. Strikingly, of all the barriers the entry into the salivary gland appears as the most formidable.

On a molecular engineering note: we first sought to use our established mutagenesis approach to alter *myoA* but found that the necessary change of the endogenous 3'UTR for the 3'UTR of *dhfs* led to decreased expression of *myoA* in early oocysts, which impacted the capacity of the sporozoites to enter salivary glands. A similar approach for the generation of MyoA-GFP readily yielded salivary gland invasion (Green *et al*, 2017). However, the produced line was not clonal and the presence of wt *myoA* in the oocysts might have produced enough MyoA to compensate for the loss due to the unnatural 3'UTR. We previously used a gene-in-marker-out approach to mutate actin, which was also based on the generation of an initial recipient line where the 3'UTR of actin 1 was replaced by the 3'UTR of *dhfs* to facilitate gene replacement (Douglas *et al*, 2018). While this parasite line acted as a recipient for further modifications in the blood stages and was thus not required for mosquito infection, a strongly reduced salivary gland entry by this modified

line was observed as well, suggesting that the expression of not only *myoA* but also *actin 1* is affected by a modified 3'UTR (Ross Douglas, unpublished). To avoid similar problems with other proteins, it might be advisable to use a gene-in-marker-out approach that leaves the 3'UTRs unaffected or a CRISPR/Cas9 system for subtle mutagenesis (Shinzawa *et al*, 2020).

Finally, we noted that it was possible to replace the *P. berghei myoA* gene for that of *myoA* from *P. falciparum*. However, the resulting parasites grew much slower in the blood and had deficits in infecting the mosquito. Multiple explanations are possible for these observations. Firstly, the *myoA* gene from *P. falciparum* was codon modified and hence the gene might not have been transcribed in sufficient amounts, as we noted recently for the gene encoding alpha-tubulin 1 (Spreng *et al*, 2019). Alternatively, the subtle differences in the amino acid sequence of the two myosins might be enough to cause the phenotype. Due to the additional problems associated with the 3'UTR, we chose not to follow up on these differences. However, this parasite line could be useful for future biochemical experiments investigating the interaction of, for example, myosin A with its light chains. We also noted small differences between the reconstituted WT parasites and WT parasites in the speed of hemolymph sporozoites and salivary gland-derived sporozoites migrating in 3D (but in no other parameter), which could potentially be attributed to the fact that the reconstituted WT parasites are clonal lines or to experimental variation. In addition, we note that we did not determine the amount of myosin in our different mutants and cannot fully exclude that some of the observed differences are due to changes in protein levels. Similarly, the use of alternative phosphorylation sites was not examined and could potentially influence the expressed mutant proteins.

In conclusion, the presented data suggest that sporozoites need S19 phosphorylation to efficiently enter mosquito salivary glands and infect the mammalian host, consistent with the observation that MyoA is phosphorylated in sporozoites (Swearingen *et al.*, 2017). Regulation of motility across the life cycle requires complex modulations according to the environmental barriers faced by the different forms of the parasites. Entry into salivary glands emerges as a strong barrier in parasite transmission which the parasites need to overcome.

## Materials and Methods

### Ethics statement

Animal experiments were performed according to FELASA and GV-SOLAS guidelines and approved by the responsible German authorities (Regierungspräsidium Karlsruhe). *Plasmodium* parasites were maintained in NMRI or Swiss mice, and transmission experiments were carried out using C57Bl/6 mice. Mice were obtained from JANVIER or Charles River Laboratories and kept in the dedicated animal facility of Heidelberg University according to current guidelines (3 mice per cage, ad libitum food and water, enrichment cages).

### Generation of mutant parasite lines

Cloning was performed using restriction enzymes or Gibson assembly. PCR fragments were amplified from genomic or plasmid DNA using the primers listed in Appendix Table S1. Transfection vectors for parasite lines PbMyoA 3'dhfs, PbMyoA-GFP 3'dhfs, and PfMyoA 3'dhfs were generated from vector Pb262 (Klug & Frischknecht, 2017). The myoA 5'UTR and 3'UTR were cloned into this vector to enable double crossover homologous recombination. GFP was fused to MyoA via a 4-amino acid alanine linker. A codon-modified version of PfMyoA, kindly provided by Jake Baum (Blake *et al.*, 2020), was cloned into the transfection vector to generate parasite line PfMyoA 3'dhfs.

For the introduction of point mutations into MyoA, a recipient line was produced from a p32 vector kindly provided by Jessica Kehrer. The myoA 5'UTR and open reading frame (ORF) were cloned into this vector to enable double crossover homologous recombination. The 5'UTR of ama1 was amplified and cloned into the vector. For the generation of parasite lines MyoA E6R, MyoA S19A, and MyoA S19D, myoA was amplified with primers that were designed to introduce the mutations and cloned into vector Pb262.

The transfection vectors were linearized via restriction digest with KpnI or BamHI and SacII before transfection. *Plasmodium berghei* ANKA parasites were used for genetic modifications. Transfection and generation of isogenic parasite lines was carried out essentially as described before (Janse *et al.*, 2006; Klug & Frischknecht, 2017). DNA was prepared using ethanol precipitation, and electroporation of purified schizonts was carried out using Nucleofactor technology (Lonza). Transfection mixtures were then injected intravenously into a mouse. Transfected parasites were positively selected with 0.07 mg/ml pyrimethamine or negatively selected with 1.5 mg/ml 5-FC added into the drinking water of the mice. Clonal parasite lines were obtained by limiting dilution. Successful mutagenesis was verified via genotyping PCR with the primers listed

in Appendix Table S2, and point mutations were additionally verified by sequencing of the modified locus.

### Mosquito infection and sporozoite isolation

*Anopheles stephensi* mosquitoes were infected and sporozoites isolated from midguts, hemolymph and salivary glands as described previously (Klug & Frischknecht, 2017). Briefly, for mosquito infections, mice were infected by intraperitoneal injection of frozen stocks (150–200 ml). After 3–5 days, the infected mice were checked for the presence of gametocytes by placing a drop of tail blood on a microscope slide followed by incubation at room temperature for 10–12 min. During this time, flagellated gametes mature and exit in a process termed exflagellation. If 1–2 exflagellation events per field were observed at 40× magnification, mice were anesthetized and fed to mosquitoes. Experiments with hemolymph and salivary gland sporozoites were performed 13- to 16- and 17- to 25-day post-mosquito infection, respectively. Oocysts were counted from dissected midguts following mercurochrome staining: Midguts were permeabilized for 20 min with 1% Nonidet P40 in PBS, stained with 0.1% mercurochrome in PBS for 30 min, mounted in a small amount of PBS, covered with a coverslip, and counted using a 10× objective on a Zeiss CellObserver microscope. Midguts and salivary glands were dissected with a pair of needles in PBS and placed on ice until further use. Sporozoites were released by gently crushing the collected organs with a plastic pestle. Sporozoites were isolated from the hemolymph by cutting the last segment of the abdomen with a syringe and flushing with RPMI (supplemented with 50,000 units/l penicillin and 50 mg/l streptomycin) by inserting a long-drawn Pasteur pipette into the lateral side of the thorax. The hemolymph was drained from the abdomen, collected on a plastic foil, and transferred to a reaction tube. Sporozoites were counted using a Neubauer chamber and total numbers extrapolated according to the dilution.

### Cell migration and invasion assays

To obtain high parasitemia for *in vitro* ookinete cultures, we induced reticulocytosis in mice by intraperitoneal administration of 200 µl phenylhydrazine (6 mg/ml in PBS) two days prior to infection of mice by intraperitoneal injection of a parasite cryostock. When mice reached high parasitemia (usually 3-day post-infection), asexual parasites were cleared by administering 30 mg/l sulfadiazine to the drinking water. Two days later, mice were bled by cardiac puncture and 500 µl blood was collected in 10 ml ookinete medium (RPMI supplemented with 20% FCS, 100 µM xanthurenic acid, and 50 µg/ml hypoxanthine, adjusted to a pH of 7.8–8.0). Parasites were incubated for 20 to 22 h at 19°C, and ookinetes were purified by density gradient (63% Nycodenz/PBS, 20 min at 200 g). Purified ookinetes were resuspended in a small volume of medium, vortexed to remove clumps and imaged on a Zeiss CellObserver microscope using a 25× objective. Movies were taken for 15–20 min at a frame rate of 15 s/frame. Ookinete motility and speed were analyzed in ImageJ using the Manual Tracking Plugin. Per line, at least four movies from three different experiments were analyzed and tracking of ookinetes was done blinded.

Sporozoite migration assays on glass or in polyacrylamide hydrogels were performed and analyzed as described before (Douglas

*et al*, 2018; Ripp *et al*, 2021). Briefly, isolated sporozoites in RPMI medium supplemented with 50,000 units/l penicillin, 50 mg/l streptomycin, and 3% bovine serum albumin (BSA) were pipetted into a 96-well optical bottom plate (Nunc) and centrifuged at 1,000 rpm for 3 min. For 3D hydrogel assays, whole infected salivary glands dissected into 30  $\mu$ l of medium were sandwiched between a glass coverslip (22  $\times$  22 mm) placed on top of a microscope slide and a hydrogel manufactured from 3% acrylamid/0.03% BIS. Imaging was performed at room temperature on an inverted Zeiss CellObserver microscope. Images were recorded every second for hemolymph sporozoites or every 3 s for salivary gland sporozoites for a total time of 3 min. Sporozoite speed was determined using the manual tracking plugin from Fiji (Schindelin *et al*, 2012) by a blinded co-author.

For invasion assays, HepG2 cells were seeded in 8-well LabTek dishes at a density of 25,000 cells/well in DMEM supplemented with 10% fetal calf serum, 1 mM glutamine, and 1% Anti-anti (Gibco) at 37°C and 5% CO<sub>2</sub>. Two days later, cells were infected with 10,000 WT or MyoA S19A sporozoites per well and investigated after fixation in ice-cold methanol 24- or 48-h post-infection. Liver stages were stained with a mouse anti-PbHsp70 antibody used at a dilution of 1:300 and an Alexa488-coupled secondary anti-mouse antibody. Cells were imaged with a Zeiss CellObserver fluorescence microscope and liver-stage size analyzed with Fiji. Cell identity was verified, and cells were checked for contamination with mycoplasma.

### Force measurements

Force experiments were performed on a Nikon Eclipse TI microscope equipped with an MMI CellManipulator with a 1,070 nm laser (8W). Sample preparation was carried out as described earlier (Quadt *et al*, 2016). In short, infected salivary glands of 3–5 mosquitoes dissected in 35  $\mu$ l of medium were smashed, flown into a self-made flow chamber and incubated for 10 min. If sporozoites were attached and motile, the chamber was washed with streptavidin-coated polystyrene beads (1.5–1.9  $\mu$ m, Kisker Biotech) in 3% BSA/RPMI. Laser trap calibration was performed with the MMI Cell Tool software by adjusting the escape force of the bead to about 30 pN. The escape force was determined by harmonic bead oscillation at the z-focus of later experiments according to the Stoke's equation with the known viscosity of the medium and bead diameter. A bead was captured at a defined laser power of 30 pN and placed onto the apical end of a moving sporozoite. The percentage of motile sporozoites that could pull the bead out of the trap toward the rear end of the sporozoite was quantified. Experiments were performed at room temperature.

### qRT-PCR

To determine expression levels of MyoA in wt and PbMyoA 3'dhfs parasites, total RNA of 15–20 mosquito midguts (day 10 post-infection) and purified schizonts (10 million parasites) was isolated with Qiazol reagent according to the manufacturer's protocol (Invitrogen). RNA was purified with the Direct-zol RNA MicroPrep kit (Zymo Research), and cDNA synthesis was generated using the First-Strand cDNA synthesis kit (Thermo Fisher Scientific) according

to the manufacturer's protocols. The quantitative PCR was performed using SYBR Green PCR Master Mix (Life Technologies) including ROX dye and was measured with the Bio-Rad CFX96 Real-Time System. The 18S rRNA gene was used as a reference, and across-run differences were normalized using a calibrator sample. Relative copy numbers were calculated by applying the  $\Delta\Delta$ Ct methodology. The sequences of the gene-specific primers used are shown in Appendix Table S3.

### Statistical analysis

Graphs were created using R. Statistical analysis was performed in R. Figures were generated using Inkscape.

## Data availability

No large primary datasets have been generated and deposited. All new vectors and parasite lines are available from the corresponding author upon request.

**Expanded View** for this article is available online.

### Acknowledgments

We thank Miriam Reing for rearing *Anopheles stephensi* mosquitoes, Joachim Spatz for access to, and Katharina Quadt for setup, calibration, and introduction of the new laser tweezers as well as Jake Baum, Ross Douglas, and Anne Houdousse for helpful discussions and comments during the project and on the manuscript. This work was funded by grants from the Human Frontier Science Program (RGY0066/2016) and the Deutsche Forschungsgemeinschaft (DFG, German Research Foundation, DFG project number 240245660—SFB 1129) and German Center for Infection Research (TTU 03.813). FF is a member of CellNetworks Cluster of excellence at Heidelberg University, and the collaborative research enters SFB 1129, SPP 2225, and SPP 2332. JR was a member of Heidelberg International Graduate School for the Biosciences (HBIGS) and XS and MTN members of the Master Program for Molecular Biotechnology at Heidelberg University. We acknowledge the essential microscopy support from the Infectious Diseases Imaging Platform (IDIP) at the Center for Integrative Infectious Disease Research. Open access funding enabled and organized by Projekt DEAL.

### Author contributions

**Johanna Ripp:** Conceptualization; Data curation; Formal analysis; Supervision; Investigation; Visualization; Methodology; Writing—original draft; Writing—review & editing. **Xanthoula Smyrnakou:** Formal analysis; Investigation. **Marie-Therese Neuhoff:** Formal analysis; Investigation; Methodology. **Friedrich Frischknecht:** Conceptualization; Supervision; Funding acquisition; Writing—original draft; Project administration; Writing—review & editing. **Franziska Hentzschel:** Data curation; Formal analysis; Investigation; Visualization; Writing—review & editing.

In addition to the CRediT author contributions listed above, the contributions in detail are:

JR and FF designed the project; JR, XS, M-TN, and FH performed research; all authors analyzed data; FF supervised the study. JR and FF wrote the paper with input from all authors.

### Disclosure and competing interests statement

The authors declare that they have no conflict of interest.



## References

- Alam MM, Solyakov L, Bottrill AR, Flueck C, Siddiqui FA, Singh S, Mistry S, Viskaduraki M, Lee K, Hopp CS *et al* (2015) Phosphoproteomics reveals malaria parasite Protein Kinase G as a signalling hub regulating egress and invasion. *Nat Commun* 6: 7285
- Aleshnick M, Ganusov VV, Nasir G, Yenokyan G, Sinnis P (2020) Experimental determination of the force of malaria infection reveals a non-linear relationship to mosquito sporozoite loads. *PLoS Pathog* 16: e1008181
- Andenmatten N, Egarter S, Jackson AJ, Jullien N, Herman JP, Meissner M (2013) Conditional genome engineering in *Toxoplasma gondii* uncovers alternative invasion mechanisms. *Nat Methods* 10: 125–127
- Angrisano F, Delves MJ, Sturm A, Mollard V, McFadden GI, Sinden RE, Baum J (2012a) A GFP-Actin reporter line to explore microfilament dynamics across the malaria parasite lifecycle. *Mol Biochem Parasitol* 182: 93–96
- Angrisano F, Tan YH, Sturm A, McFadden GI, Baum J (2012b) Malaria parasite colonisation of the mosquito midgut - placing the *Plasmodium ookinete* centre stage. *Int J Parasitol* 42: 519–527
- Bane KS, Lepper S, Kehrler J, Sattler JM, Singer M, Reinig M, Klug D, Heiss K, Baum J, Mueller A-K *et al* (2016) The actin filament-binding protein coronin regulates motility in *Plasmodium sporozoites*. *PLoS Pathog* 12: e1005710
- Baum J, Tonkin CJ, Paul AS, Rug M, Smith BJ, Gould SB, Richard D, Pollard TD, Cowman AF (2008) A malaria parasite formin regulates actin polymerization and localizes to the parasite-erythrocyte moving junction during invasion. *Cell Host Microbe* 3: 188–198
- Blake TCA, Haase S, Baum J (2020) Actomyosin forces and the energetics of red blood cell invasion by the malaria parasite *Plasmodium falciparum*. *PLoS Pathog* 16: e1009007
- Bookwalter CS, Tay CL, McCrorie R, Previs MJ, Lu H, Kremntsova EB, Fagnant PM, Baum J, Trybus KM (2017) Reconstitution of the core of the malaria parasite glideosome with recombinant *Plasmodium* class XIV myosin A and *Plasmodium* actin. *J Biol Chem* 292: 19290–19303
- Brown ME, Bridgman PC (2003) Retrograde flow rate is increased in growth cones from myosin IIB knockout mice. *J Cell Sci* 116: 1087–1094
- Bushell E, Gomes AR, Sanderson T, Anar B, Girling G, Herd C, Metcalf T, Modrzynska K, Schwach F, Martin RE *et al* (2017) Functional profiling of a *Plasmodium* genome reveals an abundance of essential genes. *Cell* 170: 260–272
- Carey AF, Singer M, Bargieri D, Thiberge S, Frischknecht F, Ménard R, Amino R (2014) Calcium dynamics of *Plasmodium berghei* sporozoite motility. *Cell Microbiol* 16: 768–783
- Churcher TS, Sinden RE, Edwards NJ, Poulton ID, Rampling TW, Brock PM, Griffin JT, Upton LM, Zakutansky SE, Sala KA *et al* (2017) Probability of transmission of malaria from mosquito to human is regulated by mosquito parasite density in naïve and vaccinated hosts. *PLoS Pathog* 13: e1006108
- Das S, Lemgruber L, Tay CL, Baum J, Meissner M (2017) Multiple essential functions of *Plasmodium falciparum* actin-1 during malaria blood-stage development. *BMC Biol* 15: 1–16
- Douglas RG, Amino R, Sinnis P, Frischknecht F (2015) Active migration and passive transport of malaria parasites. *Trends Parasitol* 31: 357–362
- Douglas RG, Nandekar P, Aktories J-E, Kumar H, Weber R, Sattler JM, Singer M, Lepper S, Sadiq SK, Wade RC *et al* (2018) Inter-subunit interactions drive divergent dynamics in mammalian and *Plasmodium* actin filaments. *PLoS Biol* 16: e2005345
- Egarter S, Andenmatten N, Jackson AJ, Whitelaw JA, Pall G, Black JA, Ferguson DJP, Tardieux I, Mogilner A, Meissner M (2014) The toxoplasma Acto-Myo motor complex is important but not essential for gliding motility and host cell invasion. *PLoS One* 9: e91819
- Frénal K, Dubremetz JF, Lebrun M, Soldati-Favre D (2017) Gliding motility powers invasion and egress in Apicomplexa. *Nat Rev Microbiol* 15: 645–660
- Frischknecht F, Matuschewski K (2017) *Plasmodium sporozoite* biology. *Cold Spring Harb Perspect Med* 7: a025478
- Gaji RY, Johnson DE, Treeck M, Wang M, Hudmon A, Arrizabalaga G (2015) Phosphorylation of a myosin motor by TgCDPK3 facilitates rapid initiation of motility during *Toxoplasma gondii* egress. *PLoS Pathog* 11: e1005268
- Ganter M, Schüller H, Matuschewski K (2009) Vital role for the *Plasmodium* actin capping protein (CP) beta-subunit in motility of malaria sporozoites. *Mol Microbiol* 74: 1356–1367
- Gilson PR, Crabb BS (2009) Morphology and kinetics of the three distinct phases of red blood cell invasion by *Plasmodium falciparum* merozoites. *Int J Parasitol* 39: 91–96
- Govindasamy K, Bhanot P (2020) Overlapping and distinct roles of CDPK family members in the pre-erythrocytic stages of the rodent malaria parasite, *Plasmodium berghei*. *Plos Pathog* 16: e1008131
- Govindasamy K, Jebiwott S, Jaijyan DK, Davidow A, Ojo KK, Van Voorhis WC, Brochet M, Billker O, Bhanot P (2016) Invasion of hepatocytes by *Plasmodium sporozoites* requires cGMP-dependent protein kinase and calcium dependent protein kinase 4. *Mol Microbiol* 102: 349–363
- Govindasamy K, Khan R, Snyder M, Lou HJ, Du P, Kudyba HM, Muralindharan V, Turk BE, Bhanot P (2018) *Plasmodium falciparum* cyclic GMP-dependent protein kinase interacts with a subunit of the parasite proteasome. *Infect Immun* 87: e00523-18
- Green JL, Wall RJ, Vahokoski J, Yusuf NA, Ridzuan MAM, Stanway RR, Stock J, Knuepfer E, Brady D, Martin SR *et al* (2017) Compositional and expression analyses of the glideosome during the *Plasmodium* life cycle reveal an additional myosin light chain required for maximum motility. *J Biol Chem* 292: 17857–17875
- Harding CR, Frischknecht F (2020) The riveting cellular structures of apicomplexan parasites. *Trends Parasitol* 36: 979–991
- Hegge S, Uhrig K, Streichfuss M, Kynast-Wolf G, Matuschewski K, Spatz JP, Frischknecht F (2012) Direct manipulation of malaria parasites with optical tweezers reveals distinct functions of *Plasmodium* surface proteins. *ACS Nano* 6: 4648–4662
- Heintzelman MB (2015) Gliding motility in apicomplexan parasites. *Semin Cell Dev Biol* 46: 135–142
- Herm-Götz A, Weiss S, Stratmann R, Fujita-Becker S, Ruff C, Meyhofer E, Soldati T, Manstein DJ, Geeves MA, Soldati D (2002) *Toxoplasma gondii* myosin A and its light chain: a fast, single-headed, plus-end-directed motor. *EMBO J* 21: 2149–2158
- Hopp CS, Chiou K, Ragheb DRT, Salman AM, Khan SM, Liu AJ, Sinnis P (2015) Longitudinal analysis of *Plasmodium sporozoite* motility in the dermis reveals component of blood vessel recognition. *eLife* 4: e07789
- Hopp CS, Kanatani S, Archer NK, Miller RJ, Liu H, Chiou KK, Miller LS, Sinnis P (2021) Comparative intravital imaging of human and rodent malaria sporozoites reveals the skin is not a species-specific barrier. *EMBO Mol Med* 13: e11796
- Janse CJ, Ramesar J, Waters AP (2006) High-efficiency transfection and drug selection of genetically transformed blood stages of the rodent malaria parasite *Plasmodium berghei*. *Nat Protoc* 1: 646–656
- Kariuki SN, Marin-Menendez A, Introini V, Ravenhill BJ, Lin Y-C, Macharia A, Makale J, Tendwa M, Nyamu W, Kotar J *et al* (2020) Red blood cell tension protects against severe malaria in the Dantu blood group. *Nature* 585: 579–583

- Klug D, Frischknecht F (2017) Motility precedes egress of malaria parasites from oocysts. *eLife* 6: e19157
- Kudryashev M, Lepper S, Baumeister W, Cyrklaff M, Frischknecht F (2010) Geometric constraints for detecting short actin filaments by cryogenic electron tomography. *PMC Biophys* 3: 6
- Lasonder E, Green JL, Grainger M, Langsley G, Holder AA (2015) Extensive differential protein phosphorylation as intraerythrocytic *Plasmodium falciparum* schizonts develop into extracellular invasive merozoites. *Proteomics* 15: 2716–2729
- Lin JW, Annoura T, Sajid M, Chevalley-Maurel S, Ramesar J, Klop O, Franke-Fayard BM, Janse CJ, Khan SM (2011) A novel 'gene insertion/marker out' (GIMO) method for transgene expression and gene complementation in rodent malaria parasites. *PLoS One* 6: e29289
- Matz JM, Kooij TWA (2015) Towards genome-wide experimental genetics in the *in vivo* malaria model parasite *Plasmodium berghei*. *Pathog Glob Health* 109: 46–60
- Meissner M, Schlüter D, Soldati D (2002) Role of *Toxoplasma gondii* myosin A in powering parasite gliding and host cell invasion. *Science* 298: 837–840
- Mizuno Y, Makioka A, Kawazu SI, Kano S, Kawai S, Akaki M, Aikawa M, Ohtomo H (2002) Effect of jasplakinolide on the growth, invasion, and actin cytoskeleton of *Plasmodium falciparum*. *Parasitol Res* 88: 844–848
- Montagna GN, Buscaglia CA, Münter S, Goosmann C, Frischknecht F, Brinkmann V, Matuschewski K (2012) Critical role for heat shock protein 20 (HSP20) in migration of malarial sporozoites. *J Biol Chem* 287: 2410–2422
- Moreau CA, Bhargav SP, Kumar H, Quadt KA, Piirainen H, Strauss L, Kehrer J, Streichfuss M, Spatz JP, Wade RC et al (2017) A unique profilin-actin interface is important for malaria parasite motility. *PLOS Pathog* 13: e1006412
- Moreau CA, Quadt KA, Piirainen H, Kumar H, Bhargav SP, Strauss L, Tolia NH, Wade RC, Spatz JP, Kursula I et al (2020) A function of profilin in force generation during malaria parasite motility independent of actin binding. *J Cell Sci* 134: jcs233775
- Moussaoui D, Robblee JP, Auguin D, Kremntsova EB, Haase S, Blake TCA, Baum J, Robert-Paganin J, Trybus KM, Houdusse A (2020) Full-length *Plasmodium falciparum* myosin A and essential light chain PfELC structures provide new anti-malarial targets. *eLife* 9: e60581
- Münter S, Sabass B, Selhuber-Unkel C, Kudryashev M, Hegge S, Engel U, Spatz JP, Matuschewski K, Schwarz US, Frischknecht F (2009) *Plasmodium sporozoite* motility is modulated by the turnover of discrete adhesion sites. *Cell Host Microbe* 6: 551–562
- Poinar G (2016) What fossils reveal. *Am Entomol* 62: 1–25
- Quadt KA, Streichfuss M, Moreau C, Spatz JP, Frischknecht F (2016) Coupling of retrograde flow to force production during malaria parasite migration. *ACS Nano* 10: 2091–2102
- Ripp J, Kehrer J, Smyrnakou X, Tisch N, Tavares J, Amino R, Ruiz de Almodovar C, Frischknecht F (2021) Malaria parasites differentially sense environmental elasticity during transmission. *EMBO Mol Med* 13: e13933
- Robert-Paganin J, Robblee JP, Auguin D, Blake TCA, Bookwalter CS, Kremntsova EB, Moussaoui D, Previs MJ, Jousset G, Baum J et al (2019) *Plasmodium* myosin A drives parasite invasion by an atypical force generating mechanism. *Nat Commun* 10: 3286
- Sato S (2011) The apicomplexan plastid and its evolution. *Cell Mol Life Sci* 68: 1285–1296
- Schindelin J, Arganda-Carreras I, Frise E, Kaynig V, Longair M, Pietzsch T, Preibisch S, Rueden C, Saalfeld S, Schmid B et al (2012) Fiji: an open-source platform for biological-image analysis. *Nat Methods* 9: 676–682
- Sebastian S, Brochet M, Collins MO, Schwach F, Jones ML, Goulding D, Rayner JC, Choudhary JS, Billker O (2012) A *Plasmodium* calcium-dependent protein kinase controls zygote development and transmission by translationally activating repressed mRNAs. *Cell Host Microbe* 12: 9–19
- Shinzawa N, Nishi T, Hiyoshi F, Motooka D, Yuda M, Iwanaga S (2020) Improvement of CRISPR/Cas9 system by transfecting Cas9-expressing *Plasmodium berghei* with linear donor template. *Commun Biol* 3: 426
- Siden-Kiamos I, Ganter M, Kunze A, Hliscs M, Steinbüchel M, Mendoza J, Sinden RE, Louis C, Matuschewski K (2011) Stage-specific depletion of myosin A supports an essential role in motility of malarial ookinetes. *Cell Microbiol* 13: 1996–2006
- Siden-Kiamos I, Louis C, Matuschewski K (2012) Evidence for filamentous actin in ookinetes of a malarial parasite. *Mol Biochem Parasitol* 181: 186–189
- Spreng B, Fleckenstein H, Kübler P, Di Biagio C, Benz M, Patra P, Schwarz US, Cyrklaff M, Frischknecht F (2019) Microtubule number and length determine cellular shape and function in *Plasmodium*. *EMBO J* 38: e100984
- Swearingen KE, Lindner SE, Flannery EL, Vaughan AM, Morrison RD, Patrapuvich R, Koepfli C, Muller I, Jex A, Moritz RL et al (2017) Proteogenomic analysis of the total and surface-exposed proteomes of *Plasmodium vivax* salivary gland sporozoites. *PLoS Negl Trop Dis* 11: e0005791
- Tang Q, Andenmatten N, Hortua Triana MA, Deng B, Meissner M, Moreno SN, Ballif BA, Ward GE (2014) Calcium-dependent phosphorylation alters class XIVa myosin function in the protozoan parasite *Toxoplasma gondii*. *Mol Biol Cell* 25: 2579–2591
- Tosetti N, Pacheco NDS, Soldati-Favre D, Jacot D (2019) Three F-actin assembly centers regulate organelle inheritance, cell-cell communication and motility in *Toxoplasma gondii*. *eLife* 8: e42669
- Vanderberg JP (1974) Studies on the motility of *Plasmodium sporozoites*. *J Protozool* 21: 527–537
- Vanderberg JP (1975) Development of infectivity by the *Plasmodium berghei* sporozoite. *J Parasitol* 61: 43–50
- Wall RJ, Zeeshan M, Katris NJ, Limenitakis R, Rea E, Stock J, Brady D, Waller RF, Holder AA, Tewari R (2019) Systematic analysis of *Plasmodium myosins* reveals differential expression, localisation, and function in invasive and proliferative parasite stages. *Cell Microbiol* 21: e13082



**License:** This is an open access article under the terms of the Creative Commons Attribution-NonCommercial-NoDerivs License, which permits use and distribution in any medium, provided the original work is properly cited, the use is non-commercial and no modifications or adaptations are made.